arXiv:1511.01743v1 [physics.plasm-ph] 5 Nov 2015

PoPe (Projection on Proper elements) for code control: verification, numerical convergence and reduced models. Application to plasma turbulence simulations

T. Cartier-Michaud,* P. Ghendrih, Y. Sarazin, J. Abiteboul, H. Bufferand, G. Dif-Pradalier, X. Garbet, V. Grandgirard, G. Latu, C. Norscini, C. Passeron, and P. Tamain
CEA/DSM/IRFM, Cadarache, 13108 Saint-Paul-Lez-Durance, France
(Dated: November 6, 2015)

The Projection on Proper elements (PoPe) is a novel method of code control dedicated to 1) checking the correct implementation of models, 2) determining the convergence of numerical methods and 3) characterizing the residual errors of any given solution at very low cost. The basic idea is to establish a bijection between a simulation and a set of equations that generate it. Recovering equations is direct and relies on a statistical measure of the weight of the various operators. This method can be used in any dimensions and any regime, including chaotic ones. This method also provides a procedure to design reduced models and quantify the ratio costs to benefits. PoPe is applied to a kinetic and a fluid code of plasma turbulence.

PACS numbers: 52.65.-y, 52.35.Ra, 05.45.Pq, 02.60.-x

Numerical simulations are routine tools addressing non-linear problems in most fields of research and industrial applications. Demonstrating their reliability is a major concern [1, 2]. PoPe (Projection on Proper elements) is design to control such numerical experiments. Code verification, namely checking that the code is solving properly the equations at hand is a straightforward requirement and a critical issue given the complexity of massively parallelized codes. This issue must also encompass numerical convergence and projection of the solution on its validity domain. This method is applied to fusion plasmas where the requirement for precise simulation support is mandatory in view of ITER nuclear experiments [3]. It is to be underlined that the method is quite general.

PoPe does not require modifying the code nor very specifics runs provided the required data is stored for PoPe post-processing. It can then also be used for in-depth analysis of the simulations, from numerical convergence to determining reduced models. PoPe also provides a series of measures that allows one quantifying the difference between numerical schemes and merits of reduced models. By many aspects it is more appropriate than the present verification standard, the Method of Manufactured Solutions (MMS) [4, 5]. In particular, it does not rely on building a target solution with relevant properties, nor does it require modifying the code to enforce these target solutions.

PoPe is represented here using non-linear simulations. As a post-processing option, this versatile tool is shown to be useful to physicists, applied mathematicians and computers scientists. The chosen examples are a pseudo-spectral fluid turbulence code [6] and a more recent semi-Lagrangian kinetic turbulence code [7]. In the former, the method is presented together with conclusive analysis of the numerical scheme and model reduction capability. In the latter, PoPe is used to verify the code but open issues regarding the numerical convergence are detected and analyzed.

*Electronic address: t.cartiermichaud@gmail.com

PoPe verification of a fluid turbulence code

PoPe is applied to TOKAM2D [6], a pseudo-spectral code of 2D plasma interchange turbulence, akin to Rayleigh-Bénard (RB) instability in neutral fluids. It evolves two fields governed by similar equations.

$$\boldsymbol{\partial_t} n = \alpha_n \{\boldsymbol{\phi}\} n + D\boldsymbol{\Delta} n + S_0 \mathbf{S_n} - \sigma_n \mathbf{P_n} \quad (1a)$$

$$\boldsymbol{\partial_t} W = \alpha_W \{\boldsymbol{\phi}\} W + \nu \boldsymbol{\Delta} W - g\boldsymbol{\partial_y} \mathbf{log}(n) - \sigma_W \mathbf{P_W} \quad (1b)$$

$$W = \boldsymbol{\Delta}\phi \; ; \;\; \{\boldsymbol{\phi}\} f = \boldsymbol{\partial_x}\boldsymbol{\phi}\boldsymbol{\partial_y} f - \boldsymbol{\partial_y}\boldsymbol{\phi}\boldsymbol{\partial_x} f \quad (1c)$$

Bold characters identify the various operators. This forced turbulence model exhibits an instability that drives the system from a diffusive transport regime, D for particle diffusion and ν for the viscous damping, to a convective transport regime governed by the Poisson bracket terms Eq.(1c). Equations (1) are normalized so that $\alpha_n = \alpha_W = -1$. The x-direction runs from the source towards the sink and is that of the effective buoyancy force proportional to g. The y-direction is periodic. The plasma model stems from the electron particle Eq.(1a) and charge Eq.(1b) balance equations. The electron density is n, ϕ is the electric potential, and the vorticity W is related to the polarization density. For RB, n is the temperature field and ϕ the stream function. The system is driven out of equilibrium by a source term $\mathbf{S_n}$ constant in y, Gaussian in x with fixed normalized width 8.5. The volumetric non-linear sink terms $\mathbf{P_n}$ and $\mathbf{P_W}$ are specific of the plasma model and account for particle and charge losses in the third direction parallel to the magnetic field, $\mathbf{P_n} = n\ \exp(\Lambda - \phi)$ and $\mathbf{P_W} = 1 - \exp(\Lambda - \phi)$, Λ being a reference value of the electric potential. The values of the various parameters used in the simulation are listed in Appendix A.

Proper implementation of the model

Let us define $Z = (n, W)$, so that the evolution equation for the i^{th} component of Z takes the general form:

$$\boldsymbol{\partial_t} Z_i \;=\; \sum\nolimits_k C^k_{Z_i} \boldsymbol{\mathcal{O}}_k(Z) \qquad (2)$$

where the operators $\boldsymbol{\mathcal{O}}_k(Z)$ are labeled by k and act on Z, and where $C^k_{Z_i}$ weighs operator k in the evolution equation of i^{th} component of Z. Given the ensemble of operators $[\boldsymbol{\mathcal{O}}]_{min} = [\boldsymbol{\mathcal{O}}_k]_{1\le k\le 8}$, the minimal ensemble of operators needed to capture Eq.(1), hence $[\boldsymbol{\mathcal{O}}]_{min} = [\boldsymbol{\{\phi\}}\, n, \boldsymbol{\Delta} n, \mathbf{S_n}, \mathbf{P_n}, \boldsymbol{\{\phi\}}\, W, \boldsymbol{\Delta} W, \boldsymbol{\partial_y log}(n), \mathbf{P_W}]$, together with the weights : $\left[C^k_n\right]_{1\le k\le 4} = [\alpha_n, D, S_0, -\sigma_n]$, $\left[C^k_n\right]_{5\le k\le 8} = [0,0,0,0]$, and: $\left[C^k_W\right]_{1\le k\le 4} = [0,0,0,0]$, $\left[C^k_W\right]_{5\le k\le 8} = [\alpha_W, \nu, -g, -\sigma_W]$. For a code solving the generic equation Eq.(2), PoPe only requires saving within the code the computed values of the field Z and its time derivative $\boldsymbol{\delta_t} Z$ (readily obtain with finite differences) at synchronized locations and times. This must be done in such a way that, using this output data, an ensemble of operators $[\boldsymbol{\mathcal{O}}]_{N_O}$ acting on Z can be computed independently. The latter calculation can readily be performed with fully verified and controlled schemes. The projection of the numerical values of $\boldsymbol{\delta_t} Z$ distributed in space and time ($N_s \times N_t$ points) on an ensemble of numerically estimated operators $[\boldsymbol{\mathcal{O}}]_{N_O}$, which includes $[\boldsymbol{\mathcal{O}}_{min}]$, then yields the sets $[p^k_{Z_i}(j)]$ where $p^k_{Z_i}(j)$ is the j^{th} projection with j ranging typically from 1 to $N_t \times N_s / N_O \gg 1$. This projection is performed by solving linear systems with the $p^k_{Z_i}(j)$ considered as unknown and $\boldsymbol{\delta_t} Z_i$ evaluated on the j^{th} subset of points as right hand side. Since the weights of the various operators $\boldsymbol{\mathcal{O}}_k$ in Eq.(2) are constant and equal to $C^k_{Z_i}$, and since the model equations must be verified at all times and all locations in space, the statistical data set $[p^k_{Z_i}(j)]$, is the Probability Density Function of numerical realizations of $C^k_{Z_i}$. Of immediate relevance are then the mean-value of the computed coefficients $c^k_{Z_i} = \left\langle p^k_{Z_i}(j) \right\rangle_j$, the characteristic error $\Delta C^k_{Z_i} = |C^k_{Z_i} - c^k_{Z_i}|$ and the data scatter evaluated by $\delta c^k_{Z_i} = \left\langle ||c^k_{Z_i} - p^k_{Z_i}(j)|| \right\rangle_j$. The verification with PoPe of the proper implementation of the operator $\boldsymbol{\mathcal{O}}_k$ in the evolution equation of Z_i is then characterized by $\Delta C^k_{Z_i}/C^k_{Z_i} \ll 1$ and $\delta c^k_{Z_i}/c^k_{Z_i} \ll 1$. Furthermore, these values quantify the error introduced when stepping from the equations to their numerical integration. TOKAM2D is verified with a run of the code performed with a small time step $\Delta t = 2^{-5}$, while the value used in production runs is $\Delta t = 1$, and a mesh comparable to a standard production mesh $N_x \times N_y = 2^8 \times 2^8$ for a box size $L_x \times L_y = 2^7 \times 2^7$. For this simulation, the most unstable mode k_y is such that $N_y/(k_y L_y) \approx 13.6$ and its growth rate is $\gamma_{k_y} \approx 7.\ 10^{-4} \ll 1$. The verification of the numerical implementation of Eq.(1a) are summarized in table I. One finds that for each operator the error ΔC^k_n is small as well as the fluctuation level δc^k_n. Furthermore,

k	$\boldsymbol{\mathcal{O}}_k$ operator	Eq.(1a) run value: C^k_n	Error: ΔC^k_n	Fluctuation level: δc^k_n
1	$\boldsymbol{\{\phi\}\, n}$	-1	$1.99\ 10^{-9}$	$3.01\ 10^{-9}$
2	$\boldsymbol{\Delta n}$	0.02	$2.23\ 10^{-11}$	$4.46\ 10^{-11}$
3	$\boldsymbol{S_n}$	0.01	$5.86\ 10^{-11}$	$1.22\ 10^{-10}$
4	$\boldsymbol{P_n}$	$-1.13\ 10^{-5}$	$6.51\ 10^{-14}$	$1.33\ 10^{-13}$
5	$\boldsymbol{\{\phi\}\, W}$	0	$3.06\ 10^{-7}$	$7.64\ 10^{-7}$
6	$\boldsymbol{\Delta W}$	0	$1.09\ 10^{-8}$	$3.21\ 10^{-8}$
7	$\boldsymbol{\partial_y Log(n)}$	0	$1.72\ 10^{-11}$	$7.02\ 10^{-10}$
8	$\boldsymbol{P_W}$	0	$1.03\ 10^{-11}$	$3.95\ 10^{-11}$

TABLE I: Verification of TOKAM2D, $N_x = N_y = 256$, $N_x/L_x = N_y/L_y = 2$ and $\Delta t = 2^{-5}$

one finds that $\delta c^k_n > \Delta C^k_n$ which means that the exact value stands in the region of maximum probability of the PDF. It is to be noted that Eqs. (1a, 1b) are coupled in the evolution scheme that is based on the analytical calculation of the eigenvectors and eigenvalues of the linearized equation. However, the computed solution of Eq.(1a) exhibits a very small dependence on the operators $\boldsymbol{\mathcal{O}}_{5\le k\le 8}$ that govern the evolution of W since their computed weight is close to zero as required. Pope thus allows one to recover with good precision the weight of the various operators of the evolution equation, the implementation of the equations is thus correct.

When analyzing the PDF of the error of the coefficients of Eq.(1a), one finds a Poisson-like distribution for the Poisson bracket $\boldsymbol{\{\phi\}}\, n$ with $\Delta C^1_n \ge 0$, compatible with a rare deviation from the exact value, while the error for the coefficient $\boldsymbol{\{\phi\}}\, W$ is more Gaussian like, which can be interpreted as a random value in the vicinity of zero. Such marked differences in the PDFs remain to be fully analyzed and understood.

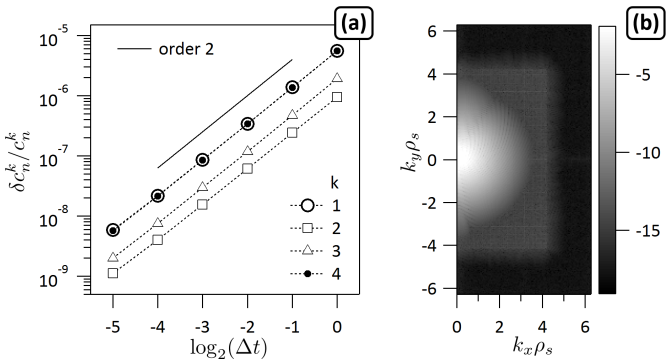

FIG. 1: (a) relative error on TOKAM2D coefficients in Eq.(1a) when scanning the time step Δt. The order 2 time integration scheme is verified. (b) 2D Fourier spectrum of $\sum_k C^k_n \boldsymbol{\mathcal{O}}_k(Z)$ on a 256×256 mesh.

Accuracy of the numerical scheme

Given the code verification, PoPe then provides a means to evaluate the accuracy of the numerical scheme. This is illustrated by computing the error $\Delta C^{1\le k\le 4}_n$ and the fluctuation level $\delta c^{1\le k\le 4}_n$, when scanning the time step Δt. The numerical evolution scheme is an order 2 predictor-corrector. It is found to be properly implemented since

one finds that the relative error $\delta c_n^k/c_n^k$ scales like Δt^2, see Fig. 1(a). The characteristic error ΔC_n^k exhibits the same dependence as the fluctuation level δc_n^k, which means that the improved matching is not governed by a change in the error statistics. Even if the C_n^k exhibits differences of several orders of magnitude, relative errors are comparable.

When analyzing the projection on operators that are absent from Eq.(1a), ΔC_n^k and δc_n^k scale like Δt^2 but the criterion $\delta c_n^k/|c_n^k| = \delta c_n^k/\Delta C_n^k$ does not. Indeed, $\delta c_n^k/c_n^k \ll 1$ identifies operators used in the equation while $\delta c_n^k/\Delta C_n^k \gtrsim 1$ identifies absent operators for which the error in determining zero and its fluctuation level are comparable.

Analysis of the residual error

Model and numerical scheme implementation verification is only complete if and only if the residual error, namely ε_i, is small. This residual error can also be analyzed for in depth control of the verification procedure, it is defined such as:

$$\varepsilon_i = \boldsymbol{\delta_t} Z_i - \sum\nolimits_k C_{Z_i}^k \boldsymbol{\mathcal{O}}_k(Z) = \mathcal{P}\varepsilon_i + (1-\mathcal{P})\,\varepsilon_i \qquad (3)$$

given $\mathcal{P}$ the projection operator on the subspace where the solution is reliable. The residual error thus addresses the error made by TOKAM2D on the time derivative $\boldsymbol{\delta_t} Z_i$. It highlights fast displacement regions with sharp changes of the magnitude of Z_i, hence fronts. The residual error is thus a measure of the error made on the front location and height, Fig. 2.

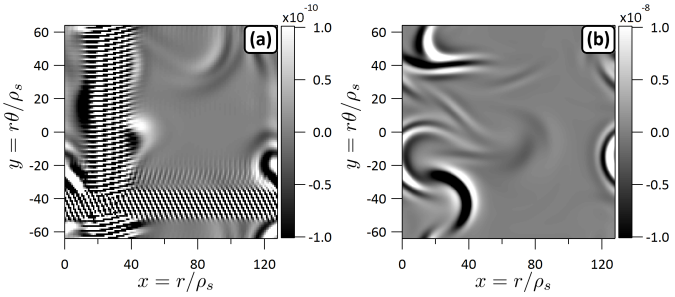

FIG. 2: Residual error ε_n Eq.(3) for two simulations, (a) 128×128, (b) enhanced resolution, 256×256.

This projection operator $\mathcal{P}$ retaining the reliable part of the solution is readily determined in pseudo-spectral codes like TOKAM2D since the de-aliasing rule sets 1/3 of the spectra at zero and is applied at each calculation of the non-linear terms. This is noticeable in the 2D space spectrum of $\sum_k C_i^k \boldsymbol{\mathcal{O}}_k(Z)$, $|\mathcal{F}(\sum_k C_i^k \boldsymbol{\mathcal{O}}_k(Z))|$, with the square shaped boundary to the region at machine precision noise Fig. 1(b). Prior to this region, one can notice a flat shoulder at the numerical noise level of the scheme ($\approx 10^{-15}$) for k-values below the cut-off. In this properly discretized example, the ill-computed output data belongs to the region where numerical noise is reached. This feature is readily seen on Fig. 3. One finds that the spectra are quite comparable for different step size in space (a), while the residual error exhibits a marked difference in shape (b). For the low resolution case, $N = 128$, the residual error exhibits a marked discontinuity at the cut-off value of the wave vector which shows that the projection $\mathcal{P}$ is removing a meaningful part of the spectrum. Conversely, for $N = 256$, the residual error exhibits a smooth decay from the numerical to the machine noise levels (b).

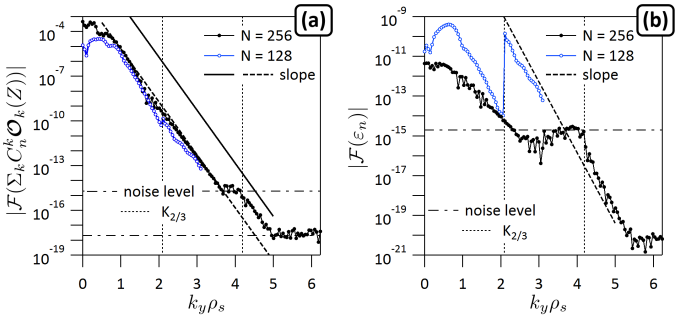

FIG. 3: (a) Fourier transform of $\sum_k C_n^k \boldsymbol{\mathcal{O}}_k(Z)$, RHS of Eq.(1a). (b): Fourier transform of residual error $\varepsilon_n = \boldsymbol{\delta_t} n - \sum_k C_n^k \boldsymbol{\mathcal{O}}_k(Z)$, RHS of Eq.(3).

In real space the residual error ε_n, Fig. 2(a), allows one identifying accuracy issues, hence for the low resolution case, $N = 128$, aliasing patterns indicate that space resolution improvement is required. Evidence of a proper discretization is given by the residual error for $N = 256$, Fig. 2(b). The residual error then exhibits a dipolar structure suggesting that the front location displacement is underestimated while its shape is properly captured. Further numerical scheme improvement is then governed by more accurate time stepping.

PoPe verification of the kinetic code TERESA

We consider here a $3D$ kinetic code, $2D$ in space, the angle ξ and the radial label ψ, and $1D$ in energy E for the various classes of particles. By many aspects, the physical model addressed by the TERESA code can be understood as a kinetic version of the Rayleigh-Bénard problem. Regarding plasma physics, it is a low frequency model of turbulence for deeply trapped particles in the harmonic oscillator regime of the tokamak confinement geometry. The equations implemented in the TERESA code are the Vlasov equation for the particle distribution function and a Poisson equation yielding the electrostatic potential.

$$\boldsymbol{\partial_t} \bar{f} = -\left(\boldsymbol{\partial_\psi} \bar{\phi} \boldsymbol{\partial_\xi} \bar{f} - \boldsymbol{\partial_\xi} \bar{\phi} \boldsymbol{\partial_\psi} \bar{f} + (\omega_D E) \boldsymbol{\partial_\xi} \bar{f}\right) \qquad (4a)$$

$$\int \boldsymbol{\mathcal{J}} \bar{f} dE - 1 = -\left(C_e \left(\phi - \lambda \langle \phi \rangle_\xi\right) - C_i \boldsymbol{\Delta_J} \phi\right) \qquad (4b)$$

where the bar quantities in Eq.(4a) are obtained from the no bar quantities by a double average on high frequency contributions to particle motion. For any given function U depending on space coordinates, it is computed as:

$$\bar{U} = \boldsymbol{\mathcal{J}} U = \left(1 - \frac{E\delta_0^2}{4} \boldsymbol{\partial_\psi^2}\right)^{-1} \left(1 - \frac{E\rho_0^2}{4} \boldsymbol{\partial_\xi^2}\right)^{-1} U \qquad (5a)$$

$$\boldsymbol{\Delta_J} = \rho_0^2 \boldsymbol{\partial_\xi^2} + \delta_0^2 \boldsymbol{\partial_\psi^2} \qquad (5b)$$

The operator $\boldsymbol{\Delta_J}$ that appears in Eq.(4b), defined in Eq.(5b), is related to the polarization of the particle trajectories during the high frequency quasi-periodic motion. Its expression is thus closely related to the averaging operator Eq.(5a).

Compare to TOKAM2D, TERESA verification is addressed here by retaining only the dependence of the relative error on the energy. The relative error of the weights of the Vlasov equation, 1, -1 for the Poisson bracket and ω_D E for the drift motion, ranges from 10^{-1} to 10^{-5}. This indicates that the model is correctly implemented. The energy dependence of the error is two-fold. Regarding the Poisson bracket terms, one finds that improving the precision allows one reducing the error. Conversely, for the ξ-convection, weight $\omega_D E$, the error remains significant with an increase towards the small values of E for solution with large convection cells (streamer solutions), see Fig. 4. This limitation is understood given the quasi-steady state solution of the TERESA model with large convection cells that generates fronts in the distribution function at the mesh resolution. These fronts are approximately aligned along constant ξ-lines and are convected in ξ. Such a behavior was not anticipated and the interpolation scheme that is presently used in the TERESA semi-Lagrangian code is not suited for such sharp front solutions. Small errors in the location of the step in the distribution value thus generates a large error that cannot be reduced since the width of the front is the mesh resolution.

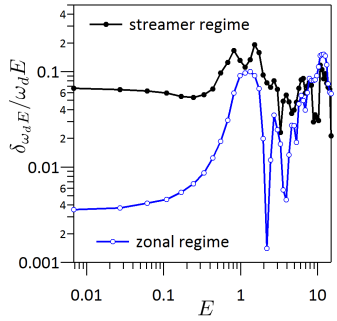

FIG. 4: Relative error of the weight $\omega_d E$ in Eq.(4a) with respect to the energy dimension.

Quantifying reduced models with PoPe

The relation established between the code output and the weight of the various operators can be used to evaluate reduced models rather than the source model as done in the verification step. Building a suit of models from first principles to operation developed in a consistent fashion will be mandatory for ITER, and even more in DEMO fusion reactors with limited diagnostics. In such a framework, one presents here the best fitting Lotka-Volterra model [8, 9] of TOKAM2D intermittent regime.

We consider TOKAM2D run in a regime with a large viscosity, and therefore with a reduced number of degree of freedom. A decrease of turbulent activity and chaos is expected [10]. In the chosen example, an intermittent behavior with periods of quasi-steady convective transport followed by rapid bursts of turbulence is observed. This governs a quasi-periodic cycle of relaxation events reminiscent of the predator prey dynamics [11]. To test the validity of this description one determines with PoPe the best set of weights of the Lotka-Volterra predator-prey model to capture this behavior. For this analysis, the code data is reduced to two fields: the prey p which is the energy of the set of harmonics of the most unstable mode of the Fourier transform of the density Eq.(1a), $p = F(n)$, and the predator P standing for the energy of all the other Fourier modes, $P = (1 - F)(n)$, see Fig. (5). From this figure one can notice that minimizing the residual error yields a Lotka-Volterra cycle that closely matches the TOKAM2D cycle. Similarly, alternative predator-prey models can then be tested.

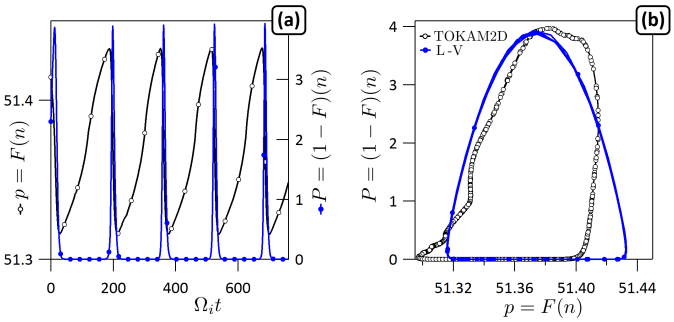

FIG. 5: (a) time trace of predator, $P = (1 - F)n$ closed symbols, prey, $p = F(n)$ open symbols. (b) Predator versus prey cycle obtained with TOKAM2D, open symbols, Lotka-Volterra reduced model determined by PoPe, closed symbols.

Summary

It is possible to numerically recover equations from a set of data, in the present case, generated by simulations. If one knows the equations to be implemented in the code, PoPe is a powerful method to monitor the accuracy of the numerical methods by studying the weights of the various operators and recovering the values that are used as simulation input. Such direct data-mining method is intrinsic conversely to benchmark verification that relies on external verification. Using the same procedure, PoPe provides a method to determine reduced models that capture a fraction of the dynamics observed in the data. From a computational point of view, this method is generic, straight forward to implement and with an overall low computational cost. Regarding plasma turbulence simulations, we have shown that a code can be verified regarding the equation implementation despite using an unoptimized numerical scheme as in the TERESA case. For the other example, TOKAM2D, good control of the simulation is achieved. This leads us to understand the results in terms of statistical distribution of the control parameters in both original and reduced models. By quantifying these statistics PoPe provide a means to adapt the simulation accuracy to a target precision.

Acknowledgments

This work was granted access to the HPC resources of Aix-Marseille Universit supported by the project Equip@Meso (ANR-10-EQPX-29-01) of the program "Investissements d'Avenir" supervised by the Agence Nationale pour la Recherche. The authors acknowledge fruitful interactions at La Maison de la Simulation (Saclay, France), the Festival de Théorie (Aix-en-Provence, France) and financial support of the A*MIDEX project "Kinetic Fluid Computing and signature in measurements" (ANR-11-IDEX-0001-02) funded by "Investissements d'Avenir".

[1] P. J. Roache. *Verification and Validation in Computational Science and Engineering*. Hermosa Publishers , Albuquerque, NM, USA, 1998. ISBN-10: 0913478083.

[2] William L. Oberkampf and Timothy G. Trucano. Verification and validation in computational fluid dynamics. *Progress in Aerospace Sciences*, 38(3):209 – 272, 2002.

[3] K. Ikeda. Progress in the iter physics basis. *Nuclear Fusion*, 47(6), 2007.

[4] Patrick J. Roache. Code verification by the method of manufactured solutions. *Journal of Fluids Engineering*, 124(1):4–10, November 2001.

[5] P. Ricci, F. Riva, C. Theiler, A. Fasoli, I. Furno, F. D. Halpern, and J. Loizu. Approaching the investigation of plasma turbulence through a rigorous verification and validation procedure: A practical examplea). *Physics of Plasmas*, 22(5):–, 2015.

[6] Y. Sarazin and Ph. Ghendrih. Intermittent particle transport in two-dimensional edge turbulence. *Physics of Plasmas (1994-present)*, 5(12):4214–4228, 1998.

[7] T. Cartier-Michaud, Ph. Ghendrih, V. Grandgirard, and G. Latu. Optimizing the parallel scheme of the poisson solver for the reduced kinetic code TERESA*. *ESAIM: Proc.*, 43:274–294, 2013.

[8] A.J. Lotka. Contribution to the theory of periodic reaction. *J. Phys. Chem.*, 14(3):271274, 1910.

[9] V. Volterra. Variazioni e fluttuazioni del numero dindividui in specie animali conviventi. *Mem. Acad. Lincei Roma*, 2:31–113, 1926.

[10] E K Maschke and B Saramito. On the transition to turbulence in magneto-hydrodynamic models of confined plasmas. *Physica Scripta*, 1982(T2B):410, 1982.

[11] P. H. Diamond and T. S. Hahm. On the dynamics of turbulent transport near marginal stability. *Physics of Plasmas (1994-present)*, 2(10):3640–3649, 1995.

Appendix A: TOKAM2D parameters

Eq.(1a)	value	Eq.(1b)	value
α_n	-1	α_W	-1
D	0.02	ν	0.01
S_0	0.01	g	$5.723\ 10^{-4}$
σ_n	$1.135\ 10^{-5}$	σ_W	$-1.135\ 10^{-5}$